Materials Horizons

ROYAL SOCIETY OF CHEMISTRY

COMMUNICATION

View Article Online
View Journal | View Issue

Check for updates

Cite this: *Mater. Horiz.*, 2025, **12**, 4444

Received 31st December 2024,
Accepted 25th March 2025

DOI: 10.1039/d4mh01929f

rsc.li/materials-horizons

Semiconducting and environmentally responsive melanin-doped silk nanofibers for multifunctional electronic tattoos†

Shalik Ram Joshi,[a] Soohoon Lee[a] and Sunghwan Kim*[ab]

On-skin electronics are gaining attention in diagnostics and therapeutics due to their capabilities such as continuous real-time operation. Among them, ultrathin electronic tattoos (E-tattoos) offer the advantage of imperceptible operation, making them suitable for daily use. However, the insulating trait of polymeric materials used for skin adhesion and integration of electronics hinders electrical interfaces between electronics and skin. This study investigates multifunctional E-tattoos by materializing semiconducting silk nanofibers (SNFs) with the melanin dopant. Fabricated through electrospinning and subsequent melanin doping and graphene coating, ultrathin and lightweight E-tattoos exhibited mechanical flexibility, strong skin conformability, and high water-vapour transmission, ensuring long-term on-skin usability. Their use as electrocardiogram electrodes and in skin hydration monitoring with a high signal-to-noise ratio is possible due to the increased conductivity of the melanin-doped SNFs. In addition, light- and humidity-responsive conductivity of melanin enables the use of E-tattoos as a breath sensor and UV detector. The unique combination of bio-based materials and advanced fabrication processes enables seamless integration of electronic and biological systems. The graphene/melanin-doped SNF E-tattoos for bio-signal sensing applications offer an eco-friendly, skin-compatible, and multifunctional solution for next-generation biomedical research.

New concepts

Biomedical diagnostics and therapeutics using on-skin electronics are attracting considerable research attention. One of the current issues facing on-skin electronics is the interface between skin and electronics. Here, we report an electronic tattoo (E-tattoo) platform where the skin-attached insulating layer is transformed into the conductivity-adjustable semiconductor layer by doping melanin into silk nanofibers (SNFs), a natural biopolymer. Melanin, a biological pigment, can regulate electrical conductivity as the melanin concentration is controlled. This implies that by imparting electrical conductivity to the insulating SNF layer between the electrode and skin, an electrical interface connection can be established. This enables high signal-to-noise ratio signal acquisition when used as an electrode patch for electrocardiography or for transdermal moisture level measurement. Its moisture and light-responsive properties in terms of conductivity make it suitable for respiratory and UV sensing applications. Integrating multifunctionality into the single E-tattoo platform is anticipated, in addition to the advantages of our silk-based E-tattoos.

1. Introduction

Merging electronics with biological tissues offers potential for diverse biomedical applications, enabling continuous and real-time diagnostics, therapeutic interventions, and human–machine interactions.[1–5] In particular, continuous tracking of biological signals in everyday life is vital for the early detection of illness symptoms and monitoring subtle changes in physical conditions.[6] Among many human tissues, the skin serves as a critical barrier between the internal environment and external surroundings, while also acting as a conduit connecting the internal body with the external environment. Hence, it is possible to acquire important bioinformation *via* the skin. For example, sweat released from the skin contains chemical substances with bioactive information, and bioelectric currents can be measured through the skin surface *via* electrocardiography (ECG) or electromyography, which indirectly provides information about the functioning of internal organs.[7,8] Therefore, measuring bioinformation with no harm to the skin is becoming increasingly important. However, conventional medical devices that measure this information are based on rigid probes that require firm contact with the skin, making them unsuitable for continuous monitoring in daily life.[9,10] These probes often cause discomfort and can lead to skin irritation due to bacterial growth resulting from sweat accumulation. To address these challenges, thin, skin-adherent electrodes

[a] *Department of Electronic Engineering, Hanyang University, Seoul 04763, Republic of Korea. E-mail: skim81@hanyang.ac.kr*
[b] *Department of Biomedical Engineering, Hanyang University, Seoul 04763, Republic of Korea*

† Electronic supplementary information (ESI) available. See DOI: https://doi.org/10.1039/d4mh01929f

that measure skin hydration without applying pressure are highly desirable.

Unlike traditional rigid electronics, epidermal electronic tattoos (E-tattoos) provide a flexible, skin-compatible alternative capable of seamlessly interfacing with biological tissues.[11–13] For skin compatibility, soft and flexible bio-friendly materials are essential. While polymeric biomaterials such as poly(dimethylsiloxane),[14–16] polyimide,[17] poly(l-lactide-*co*-glycolide),[18] and poly(ethylene terephthalate)[19] have been explored, there are still challenges related to embedding flexible electrodes into cost-effective, biocompatible, and adaptable substrates. The conventional fabrication of these materials often involves resource intensive processes and the use of toxic substances, prompting a global shift towards sustainable and eco-friendly practices.[20] Bio-based byproducts have recently been explored as a means of enhancing sustainability, albeit with occasional trade-offs in device performance.[21] Silk protein extracted from the *Bombyx mori* cocoon has been widely utilized in the textile industry and is now gaining recognition as an electronic and optical material for biomedical applications due to its biocompatibility, optical transparency, and micro/nanofabrication capabilities.[22–25] Various silk-based electrical and optical devices,[23] such as sensors for food,[26] health monitoring,[11] and wearable electronics,[11] have been demonstrated for biomedical and environmental applications. In E-tattoo applications, the nanofiber (NF) form of silk protein shows the potential to be an all-around player by providing strong skin adhesion, biocompatibility, breathability, and deformability at the same time. However, due to its insulating nature and limited mechanical resilience, it is required to incorporate conductive fillers into silk to improve its properties. Furthermore, silk nanofibers (SNFs) require additional chemical treatment for crystallization, making them resistant to water.[27]

Although several inorganic materials have been used to enhance moisture sensitivity,[28] the use of biomolecules in electrical devices remains an active area of research.[29] Inorganic materials such as metal oxides,[30] transition metal dichalcogenides,[31] and carbon-based nanomaterials[32] have been widely investigated for their ability to detect humidity through changes in electrical resistance, capacitance, or surface charge effects. These materials rely on the adsorption and desorption of water molecules on their surfaces, which induces variations in charge carrier density or dielectric properties, thereby enabling humidity sensing. While inorganic materials have demonstrated effectiveness in humidity sensing, their limitations in terms of mechanical rigidity, biocompatibility, signal stability, and adaptability to epidermal applications create challenges for their direct use in wearable bioelectronics. Melanin, a natural dark pigment, exhibits exceptional broadband light absorption and hybrid electronic–ionic conductivity, enabling critical biological functions such as photoprotection and free radical scavenging.[33] The unique properties of melanin, including hydration-dependent conductivity, amorphous semiconducting behaviour, and photoconductivity, make it an attractive material in bioelectronics.[33–35] Melanin's oligomeric and polymeric species, such as 5,6-dihydroxyindole (DHI), contribute to its efficient light absorption and unique electronic properties.[34] Early studies identified melanin as a p-type amorphous semiconductor, while more recent research attributes its electrical properties to protonic conduction under hydrated conditions.[36] However, melanin alone is insufficient for high-conductivity applications, such as measuring electrophysiological signals from the human body with a high signal-to-noise ratio.

Here, we report a skin-compatible and multifunctional E-tattoo based on a composite of melanin, SNFs, and graphene. SNFs act as a flexible biocompatible template for E-tattoo fabrication, while melanin is incorporated through an immersion-based doping process, where its concentration and immersion time are carefully controlled to achieve tunable electrical properties, making it suitable for bioinspired optoelectronic devices. The melanin–silk hybrid is ultrathin, lightweight, and highly porous and exhibits strong skin adhesion, mechanical robustness, and excellent compatibility with the skin. The addition of graphene imparts favourable electrical and thermal properties, resulting in an E-tattoo with a high conductivity of $\sim$0.12 S cm^{-1} that remains stable under mechanical deformation. The graphene/melanin-doped SNF E-tattoo has high breathability, related to high water-vapour transmission, and excellent skin conformability. The adjustable electrical properties of melanin have enabled the E-tattoo to effectively monitor skin hydration by detecting variations in skin impedance. Additionally, the photo-responsive charge generation of melanin offers a UV light detector function, where the electrical current is increased by light illumination with a photoresponsivity (I_p) of $\sim$65.7 nA W^{-1}. The E-tattoo platform leverages melanin's high reactivity towards water molecules and the superior electrical conductivity of graphene to operate as both a breathing sensor and a heart-rate monitoring device. Designed to align with the biological, mechanical, and electrical properties of the skin, this multifunctional E-tattoo offers a promising foundation for advanced bioelectronics, enabling seamless integration between biological and electronic systems.

2. Results and discussion

The graphene/melanin-doped SNF E-tattoo platform shows multifunctional capabilities for biomedical applications including skin hydration monitoring, UV detection, respiration sensing, and low noise electrophysiological signal measurement (Fig. 1). As shown in Fig. 1a, the fabrication process starts with SNF preparation *via* electrospinning, a cost-effective and versatile method for producing polymeric nanofibres.[29] Electrospinning requires a solution with sufficient viscosity to form a stable Taylor cone and prevent fibre breakage. To achieve this, 5 wt% poly(ethylene oxide) (PEO) was added to the silk solution at a 1 : 1 volumetric ratio. During the process, a charged jet of the solution was ejected from the Taylor cone when the applied voltage surpassed the surface tension, forming SNFs that accumulated as a web after solvent evaporation. Post-spinning, the SNF mat was treated with methanol to ensure water resistance and then doped with melanin.

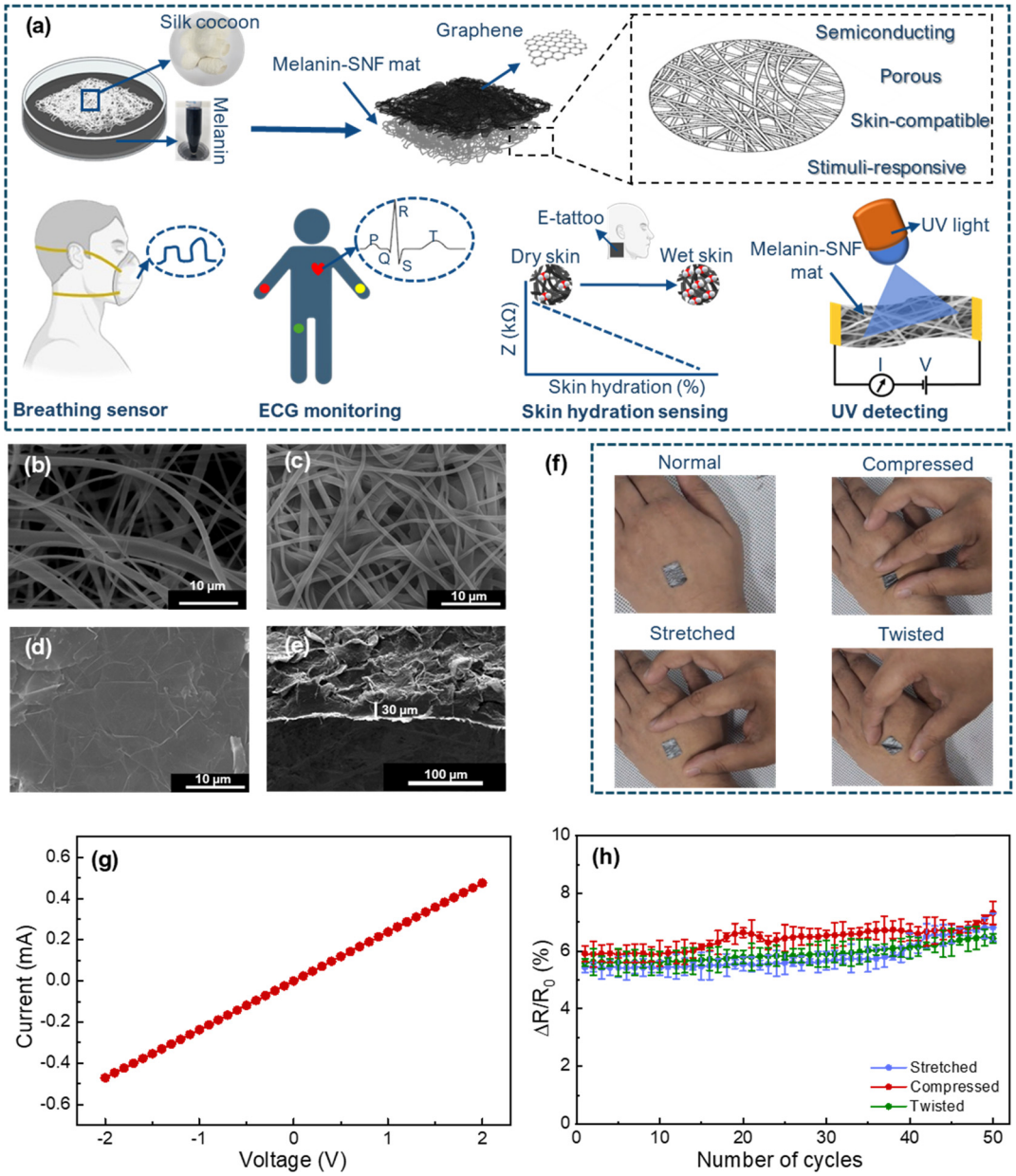

Fig. 1 Multifunctional graphene/melanin-doped SNF E-Tattoo. (a) Schematic illustration showing the fabrication and potential applications of the graphene/melanin-doped SNF mat. SEM images of the (b) bare SNF mat, (c) melanin-doped SNF mat, and (d) graphene/melanin-doped SNF E-tattoo platform. (e) Cross-sectional SEM image of the E-tattoo platform showing its thickness. (f) Optical image demonstrating the E-tattoo's stability when attached to the skin and subjected to stretching, compression, and twisting. (g) *I*–*V* curve illustrating the in-plane current flow of the E-tattoo platform. (h) Resistance variation across fifty mechanical deformation cycles, highlighting the platform's durability.

To investigate the effect of the melanin dopant on the electrical performance, melanin solutions with different concentrations (0.1 wt%, 0.5 wt%, 1 wt%, 2 wt%, and 4 wt%) were utilized to dope the melanin into SNFs. Beyond a concentration of 4 wt%, partial aggregation in solution occurred due to the reduced repulsive force, limiting the homogeneous dispersion of melanin. To evaluate the effect of immersion time on the electrical properties of the melanin-doped SNF platform, durations ranging from 0.5 h to 24 h were analyzed (Fig. S1, ESI†), as electrical conductivity is critical for enhancing signal sensitivity while minimizing background noise and instability. A 1 cm × 1 cm sample was used for current measurements, with silver paste applied to establish electrical connections. As shown in Fig. S1 (ESI†), the current increases with extended immersion time, stabilizing after 20 h. At 24 h, the current rises from ~0.1 nA to ~11.4 nA as the melanin concentration increases from 0.1 wt% to 4 wt%. Based on these findings, an immersion time of 24 h and a melanin concentration of 4 wt% were identified as the optimal conditions for sample preparation, ensuring maximum current for improved signal acquisition.

While melanin improved conductivity, it is insufficient for effective skin impedance and electrophysiological signal measurement. Thus, the graphene ink was introduced as an electrode material. The graphene ink, prepared by dispersing few-layered graphene in methanol with the sodium lauryl sulphate (SLS) surfactant to prevent agglomeration, was uniformly applied to the melanin-doped SNF mat. Only a single coating was applied, as an excessively thick graphene layer could compromise the breathability of the E-tattoo platform, a factor that will be discussed later. Scanning electron microscopy (SEM) was conducted to examine the uniform distribution of graphene on the melanin-doped SNF mat. As shown in Fig. S2 (ESI†), the low-magnification SEM image illustrates a well-coated surface, while higher-magnification images provide further evidence of a smooth and continuous graphene layer, free from noticeable agglomeration or coating inconsistencies. This even distribution plays a vital role in maintaining stable electrical conductivity and efficient charge transport within the nanofiber matrix, thereby enabling reliable electrophysiological signal detection. The resulting ultrathin, conductive E-tattoo patch offers advantages such as biocompatibility, deformability, and skin adhesiveness, overcoming limitations associated with materials like silver and gold nanowires (*e.g.*, oxidation, corrosion, and cost).[37,38] The ultrathin nature could be confirmed by weight measurements of samples with dimensions of 1 cm × 1 cm: ~3.5 mg for the bare SNF mat, ~3.8 mg for the melanin-doped SNF mat, and ~4.1 mg for the graphene/melanin-doped SNF E-tattoo, corresponding to an areal density of ~4100 μg cm^{-2}, which is significantly lower than those of previously reported epidermal E-tattoos.[1,39] The lightness enables imperceptible operation on the skin surface.

SEM images show the interconnected network of NFs (200–350 nm in diameter) in the bare SNF mat and uniform melanin deposition within the porous network (Fig. 1b and c). Graphene uniformly coated the surface, partially filling voids and forming a conductive layer, as shown in Fig. 1d and Fig. S2 (ESI†). Cross-sectional SEM analysis showed an ultrathin thickness of ~30 μm (Fig. 1e). Electrical conductivity measurements revealed the ohmic electrical response (a conductivity of ~0.12 S cm^{-1}) of the E-tattoo, confirming its suitability for electrical applications (Fig. 1f). The conformal skin attachment was facilitated by the interaction of silk's hydroxyl (–OH) and amine ($–NH_2$) groups with functional groups of the skin surface through van-der Waals bonding,[11,40] allowing integration on uneven surfaces (Fig. 1g and Video S1, ESI†). The ultrathin structure of the E-tattoo enhances intimate contact with the skin's microtopography, maximizing intermolecular interactions and ensuring stable adhesion without the need for conductive gels or additional adhesives. During the initial application, a small amount of water assists the adhesion process by softening the nanofiber matrix, allowing it to conform closely to the skin. As the water evaporates, van der Waals forces become the dominant adhesive mechanism, maintaining flexibility and breathability while ensuring prolonged attachment.[11] The E-tattoo remains securely affixed even under mild perspiration and natural skin movements, making it well-suited for long-term, non-invasive bioelectronic applications. To further evaluate its on-skin stability and adhesion, a peeling test was conducted by applying adhesive tape onto the attached E-tattoo and subsequently peeling it off (Fig. S3, ESI†). After multiple affixing–peeling cycles, the E-tattoo remained intact on the skin, demonstrating strong adhesion and durability for reliable, long-term on-skin monitoring. The E-tattoo maintained structural and functional integrity under mechanical deformations (stretching, compression, and twisting), with resistance variations below 8% across fifty cycles (Fig. 1h). These results demonstrate its stability and functionality as a bioelectronic epidermal system for advanced applications.

The chemical interactions among graphene, melanin, and SNFs were investigated using the Fourier-transform infrared (FTIR) spectroscopy method (Fig. 2a). The pure silk protein in the SNFs exhibited several characteristic peaks: a broad absorption peak around ~3300 cm^{-1} (N–H stretching, amide groups), ~1620 cm^{-1} (amide I, C═O stretching), ~1515 cm^{-1} (amide II, N–H bending), and ~1230 cm^{-1} (amide III, C–N stretching).[11,22] For the melanin-doped SNF mat, although no distinct new peaks were observed, the systematic peak shift as the melanin concentration was increased indicates homogeneous melanin dispersion without agglomeration (Fig. S4, ESI†). This systematic peak shift in the FTIR spectra provides strong evidence of the stable attachment of melanin onto the SNF mat. The observed shift in the amide peaks towards lower wavenumbers suggests enhanced hydrogen bonding interactions between melanin and the silk fibroin matrix.[41] Silk fibroin contains functional groups such as hydroxyl (–OH), carboxyl (–COOH), and amide (–CONH–) groups, which can form strong hydrogen bonds with the amine, hydroxyl, and carboxyl groups in melanin. This interaction stabilizes melanin within the nanofiber structure, preventing its detachment under dynamic conditions. After graphene coating, additional peaks appeared at ~1770 cm^{-1} and ~1900 cm^{-1}, corresponding to C═O stretching vibrations.[42] The intrinsic features of melanin were slightly suppressed due to the high graphene concentration and the shift toward lower wavenumbers indicates interactions between graphene's π-electron system and melanin's aromatic groups.[43]

UV-visible (UV-vis) spectroscopy was also used to evaluate the binding interactions between melanin and the SNF matrix (Fig. 2b). The bare SNF mat showed an optical transmission of ~23.7% at 400 nm (visible region) and ~27.4% at 800 nm (NIR region) (Fig. S5a, ESI†). Incorporating 0.1 wt% melanin reduced the transmission to ~10.9% at 400 nm and ~25.3% at 800 nm. A sharp decline of transmission was observed with higher melanin concentrations, reaching ~0.5% at 400 nm and ~0.7% at 800 nm for 4 wt% melanin (Fig. S5b, ESI†). This significant reduction was attributed to melanin's absorption characteristics, scattering from the nanofiber structure, and the optical properties of silk. These results align with the platform's suitability for UV and visible light blocking applications.

To investigate the mechanical properties, the tensile properties of the bare SNF mat, the melanin-doped SNF mat, and the graphene/melanin-doped SNF E-tattoo were evaluated by

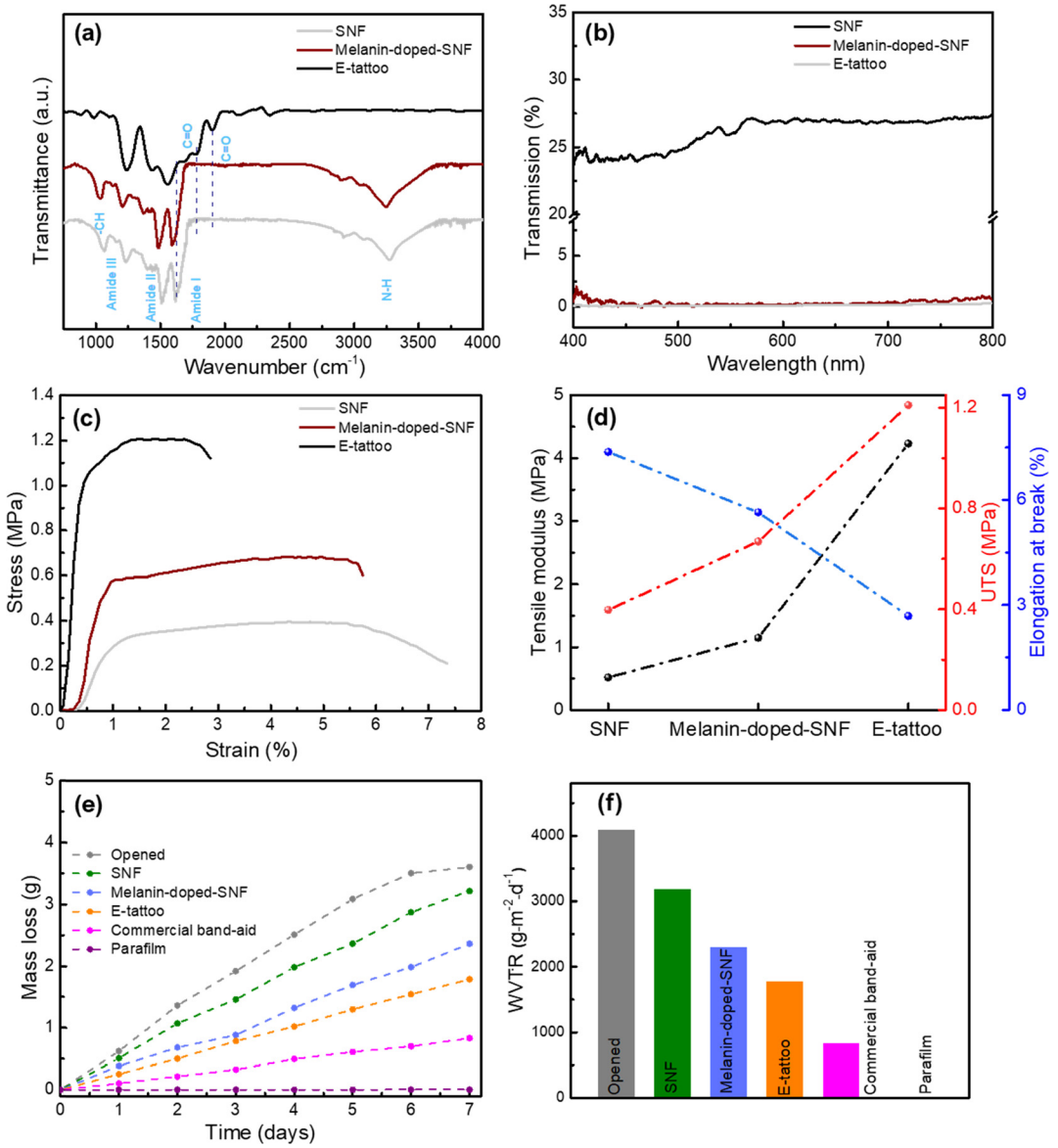

Fig. 2 Physicochemical and breathability properties of the E-tattoo. (a) FTIR spectra illustrating the chemical bonding characteristics. (b) Optical transmission spectra showing its light blocking properties. (c) Stress–strain curve and (d) tensile modulus, UTS, and elongation percentage to demonstrate the mechanical properties of SNFs, melanin-doped SNFs, and the E-tattoo platform, respectively. (e) Water loss as a function of time and (f) comparison of the WVTR of the E-tattoo platform with those of commercial band-aids and parafilm.

measuring stress–strain curves (Fig. 2c). The bare SNF mat exhibited an ultimate tensile strength (UTS) of 0.39 MPa and a tensile modulus (TM) of 0.51 MPa. Incorporating melanin increased the UTS and TM to 0.67 MPa and 1.14 MPa, respectively, at a melanin concentration of 4 wt% (Fig. S6, ESI†). However, the elongation at break decreased with higher melanin content due to melanin's rigidity, which reduced the fibre elasticity and flexibility (Fig. S6b, ESI†). Aggregates formed at higher concentrations disrupted the silk's molecular structure, creating stress concentration points that led to premature failure.[44] After graphene coating, the UTS and TM increased significantly to 1.20 MPa and 4.2 MPa, respectively (Fig. 2d). This enhancement was attributed to graphene's exceptional mechanical reinforcement and uniform dispersion and the formation of interfacial hydrogen bonding between melanin and SNFs, which improved the stress distribution and reduced defects.[45] The strong intermolecular interactions further enhanced stiffness and rigidity while the elongation at break decreased (Fig. 2d).

To assess the reusability of the E-tattoo platform, its adhesive properties were evaluated by measuring the peel forces required for detachment from pigskin, a commonly used human skin surrogate. The 90° peel test was conducted,[40] where the E-tattoo was applied to the skin and incubated for 30 min to ensure conformal adhesion. As shown in Fig. S7 (ESI†), at a low displacement (~5 mm), the E-tattoo exhibited

strong adhesion ($\sim$3.4 N m^{-1}), comparable to previously reported values.[46–48] This high adhesion is primarily attributed to the large surface area, nanoscale porosity, and flexibility of the SNF mat, which facilitates intimate contact with the skin's irregular texture.[11,47] After the second cycle, a >25% reduction in adhesion was observed, likely due to factors such as skin oil, sweat, and mechanical stress during wear and removal. Despite this limitation, silk protein-based nanofibers offer significant advantages, including biocompatibility, breathability, and excellent mechanical adaptability, which ensure comfortable, irritation-free adhesion and make silk an ideal substrate for wearable bioelectronics, promoting seamless skin interaction and long-term user comfort.

For long-term imperceptible operation of the E-tattoo, the breathability of the device is crucial, which could be assessed through measuring water vapour transmission rates (WVTRs). The WVTRs for three membranes (bare SNFs, melanin-doped SNFs, and graphene/melanin-doped SNFs) with the same thickness of $\sim$30 μm were compared to those of commercial films such as parafilm ($\sim$50 μm thick) and band-aids ($\sim$50 μm thick) (Fig. 2e). The melanin dopant reduced the WVTR to 2311 g m^{-2} d^{-1} from a value of 3191 g m^{-2} d^{-1} for the bare SNF mat. It is important to highlight that the graphene coating plays a critical role in maintaining breathability, as excessive loading can lead to denser structures that may hinder permeability. To optimize the graphene deposition on the melanin-doped SNF mat, the number of coating cycles was systematically varied. A 5 h interval was maintained between successive coatings to allow the graphene ink to dry properly before the next application. As shown in Fig. 2f, the water vapor transmission rate (WVTR) of the single-coated E-tattoo platform was $\sim$1783 g m^{-2} d^{-1}. However, with additional graphene coatings, the WVTR decreased to $\sim$693 g m^{-2} d^{-1} (Fig. S8, ESI†), likely due to the formation of a denser graphene network with repeated layering. Notably, all WVTR values of the single-coated E-tattoo platform were higher than those of commercial band-aids (Table S1, ESI†). Based on these findings, a single coating of graphene was selected for the melanin-doped SNF mat to fabricate the E-tattoo platform, ensuring an open graphene network that does not significantly obstruct the nanofiber porosity. This optimized structure enables high water vapor and oxygen permeability, which is crucial for on-skin bioelectronic applications, while preventing tissue discomfort.

The high WVTR, electrical conductivity, skin compatibility, and ultrathin design of the proposed E-tattoo platform enable continuous skin hydration monitoring without hindering transdermal water loss or causing discomfort over extended periods. The humidity-dependent conductivity of melanin plays a key role in impedance measurement, making it suitable for detecting skin hydration levels. A schematic of the E-tattoo attached to the skin for hydration monitoring is shown in Fig. 3a, illustrating its conformal attachment *via* van der Waals forces.[11] The graphene layer contributes to the platform's high electrical conductivity (electrode) and mechanical durability during use. The equivalent circuit for the E-tattoo-skin interface, depicted in Fig. 3b, models the impedance behaviour under an input signal. In this circuit, R_G represents the resistance of the graphene electrode. R_M and C_M are the resistance and capacitance of the graphene/melanin-SNF E-tattoo platform, respectively, while R_S and C_S are relevant to the stratum corneum, and R_{Deep} indicates the resistance of the deeper tissue (*e.g.* epidermis and dermis).

To evaluate the platform's hydration sensing capability, the E-tattoo was attached to pigskin as a model and its impedance was measured under varying AC bias frequencies (Fig. 3c). Impedance measurements were performed for wet and dry E-tattoos. In the wet state, water molecules containing ions OH^- and H_3O^+ improved the electrical conductivity at the electrode–skin interface, enabling better charge transport. At 100 Hz, the impedance of the wet-state E-tattoo was 6.8 ± 1.52 kΩ, whereas the dry-state impedance was significantly higher at 52.6 ± 5.4 kΩ, attributed to reduced conductivity and capacitance. Both states showed decreasing impedance with increasing bias frequency, consistent with reported trends.[49–51] To test the stability, the impedance of fully hydrated pigskin was monitored for 7 days (Fig. S9, ESI†). At 100 Hz, the impedance values remained nearly constant with less than 10% variation, indicating strong interactions between graphene and the melanin-doped SNF mat. Impedance measurements over time during skin drying (Fig. 3d) revealed an increase in impedance, confirming the platform's ability to detect moisture differences under the skin.

Human trials were conducted by applying the E-tattoo to four body parts: the forehand (Fig. S10a, ESI†), neck (Fig. S10b, ESI†), foot (Fig. S10c, ESI†), and palm (Fig. S10d, ESI†). The impedance values differed among the body parts due to variations in local skin humidity. At 100 Hz, the impedance values for the forehand, neck, palm, and foot were 45.3 ± 5.4 kΩ, 31.4 ± 3.8 kΩ, 15.7 ± 6.2 kΩ, and 10.8 ± 4.8 kΩ, corresponding to measured moisture levels of 15%, 38%, 55%, and 80%, respectively (Fig. 3e). The negative correlation between impedance and skin hydration levels demonstrates the platform's capability to monitor hydration effectively, confirming its potential for real-world applications in skin health assessment.

Due to the hygroscopic nature of melanin, environmental humidity can influence skin hydration measurements. To ensure precise monitoring for real world applications, a calibration equation was derived to mitigate these effects. For this, the E-tattoo platform was initially placed on a glass slide, and impedance at 100 Hz was measured across different humidity levels, serving as a control to assess and correct for environmental humidity interference. Subsequently, the E-tattoo platform was applied to pigskin, maintained at a stable moisture level of $\sim$40%, and impedance measurements were recorded while varying ambient humidity. As shown in Fig. S11 (ESI†), the impedance values exhibited a linear relationship with relative humidity (%RH), prompting the use of linear regression analysis to determine the calibration equation (Appendix-A). The correction process involved estimating the expected dry impedance at various humidity levels and implementing a compensation method to isolate the actual skin hydration response.

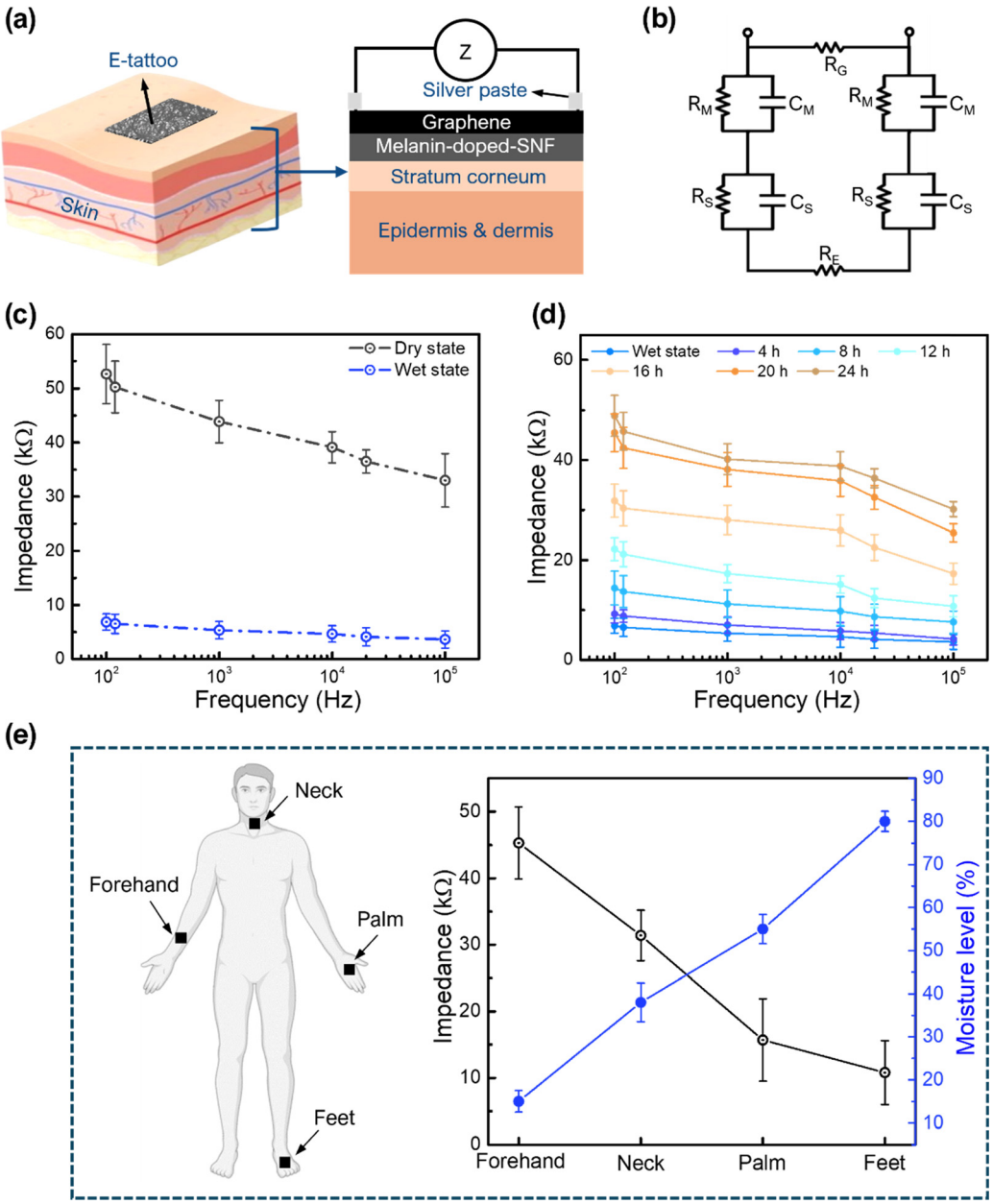

Fig. 3 Skin hydration monitoring using the graphene/melanin-doped SNF E-Tattoo. (a) Schematic representation of the impedance measurement setup for measuring skin impedance. (b) Equivalent circuit model for the E-tattoo and model skin. (c) Pigskin impedance measurement (both in dried and fully wet states) using the E-tattoo platform. (d) Pigskin impedance measurement as a function of time. (e) Skin impedance at 100 Hz frequency across the forehand, neck, foot, and palm of the human body using the E-tattoo platform. The moisture level obtained using a commercial moisture sensor is also plotted for comparison.

Additionally, the incorporation of melanin expands the platform's functionality beyond hydration monitoring to include UV detection, utilizing melanin's intrinsic light-responsive properties. Prolonged UV radiation exposure can adversely affect skin health, leading to sunburn, premature aging, and an elevated risk of skin cancer.[52] By integrating melanin, this platform gains enhanced capability for real-time UV monitoring, allowing users to track their exposure levels and adopt preventive measures to safeguard their skin. To evaluate the potential, the melanin-doped SNF mat with two silver paste electrodes was exposed to 365 nm LED light (Fig. 4a). The melanin-doped SNF mat size was maintained at 1 cm × 1 cm throughout the experiment and the photocurrent was measured in the lateral mode configuration. To assess the real time response to UV illumination, current–time (C–T) curves were recorded by repeated on–off switching of the UV-LED. As shown in Fig. 4b, the melanin-doped SNF membrane showed a clear UV light response, with a notable increase of current under UV exposure. Furthermore, the output current increased proportionally with the power density of the UV LED. The average

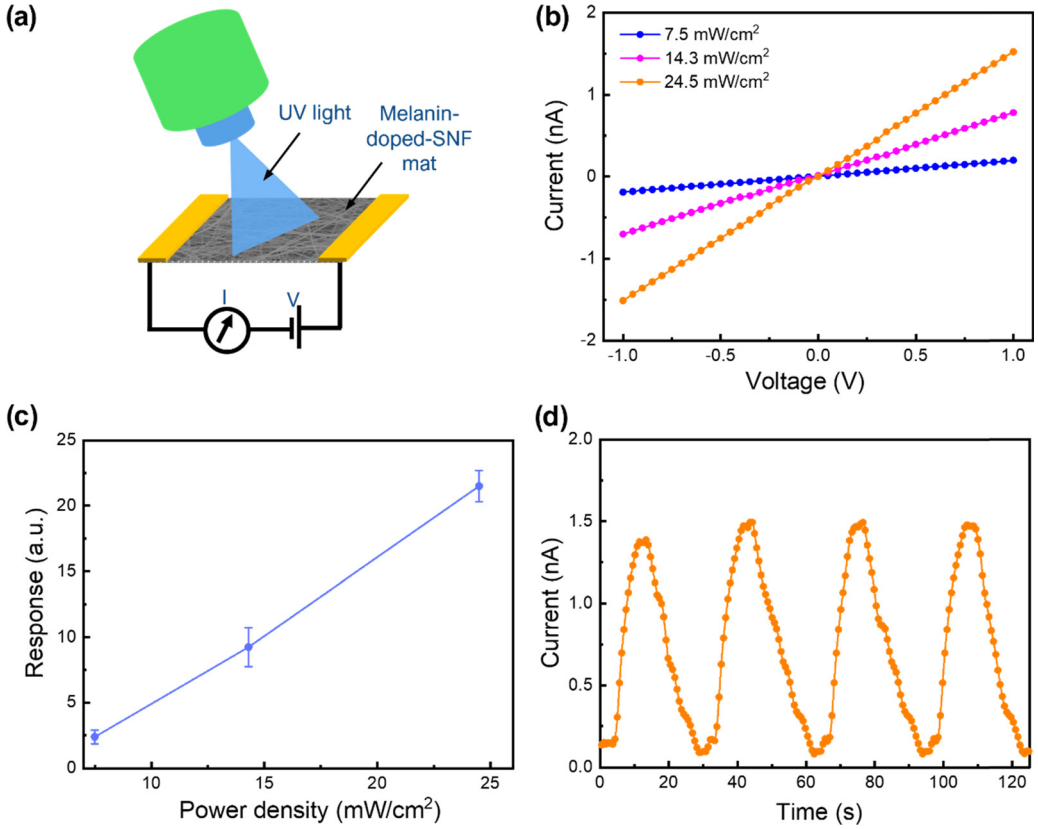

Fig. 4 Melanin-doped SNF mat for UV light detection. (a) Schematic diagram illustrating the experimental setup for monitoring current variation under UV illumination. (b) *I*–*V* curve depicting the current variation with increasing UV LED power density. (c) Response variation as a function of the UV LED power density (statistical analysis performed on n = 5 samples). (d) Reproducibility of the melanin-doped SNF mat as a UV photodetector when the membrane was exposed to the UV LED with a power density of 24.5 mW cm^{-2}.

currents were calculated to be ~0.2 nA, ~0.7 nA, and ~1.5 nA at power densities of ~7.5 mW cm^{-2}, ~14.3 mW cm^{-2}, and ~24.5 mW cm^{-2}, respectively. The response characteristics of the melanin–SNF membrane-based photodetector were calculated using the following formula:

$$\text{Response} = \frac{I_{ON}}{I_{OFF}} \quad (1)$$

where I_{ON} and I_{OFF} are the currents measured when the sample was exposed to the UV LED and in the dark, respectively. As shown in Fig. 4c, the photodetector exhibited excellent linearity, with a sensitivity of approximately ~0.53 mW cm^{-2}. This linear response indicates that the melanin–SNF membrane photodetector effectively converts UV light into electrical signals, making it a promising candidate for flexible UV photodetector applications. Additionally, the response (τ_{ON}) and recovery (τ_{OFF}) times of the melanin–SNF membrane photodetector were observed to be ~6.6 s and ~16.5 s, respectively (Fig. S12, ESI†), which are comparable to previously reported nanofiber-based photodetectors (Table S2, ESI†). The rapid response results from efficient photon absorption and swift photoexcitation of charge carriers, while the slower recovery is attributed to delayed recombination of carriers, surface trapping, and environmental factors like adsorption/desorption of molecules. Additionally, the intrinsic properties of the nanofibers, such as charge mobility and surface defects, alongside thermal effects and gradual relaxation to baseline conditions, further prolong the recovery process.[53,54] These results highlight the membrane's potential as a UV photodetector, offering efficient charge carrier generation, linear sensitivity, and stable response characteristics, making it suitable for a wide range of optoelectronic applications.

One interesting property of melanin is that its electrical conductivity can be regulated by the moisture level, which is related to the potential application of our E-tattoo as a humidity sensor. The humidity-sensing capability of the melanin-doped SNFs was evaluated by measuring the electrical current at various relative humidity (RH) levels (2–75%) and at a constant temperature of 25 °C. Measurements were conducted using five different sensors to ensure statistical reliability. The current increased with increasing humidity (Fig. 5a), with distinct behaviours observed in low (2–11%) and high (23–75%) humidity regions (Fig. 5b). At low humidity, the current increased linearly with a sensitivity of ~0.79 ± 0.04 nA/% RH, primarily due to electronic conduction driven by melanin's semiconducting properties.[36] Limited water adsorption in this range leads to isolated water molecules, restricting protonic conduction.[36] Beyond 11% RH, the current rose sharply, with a sensitivity of

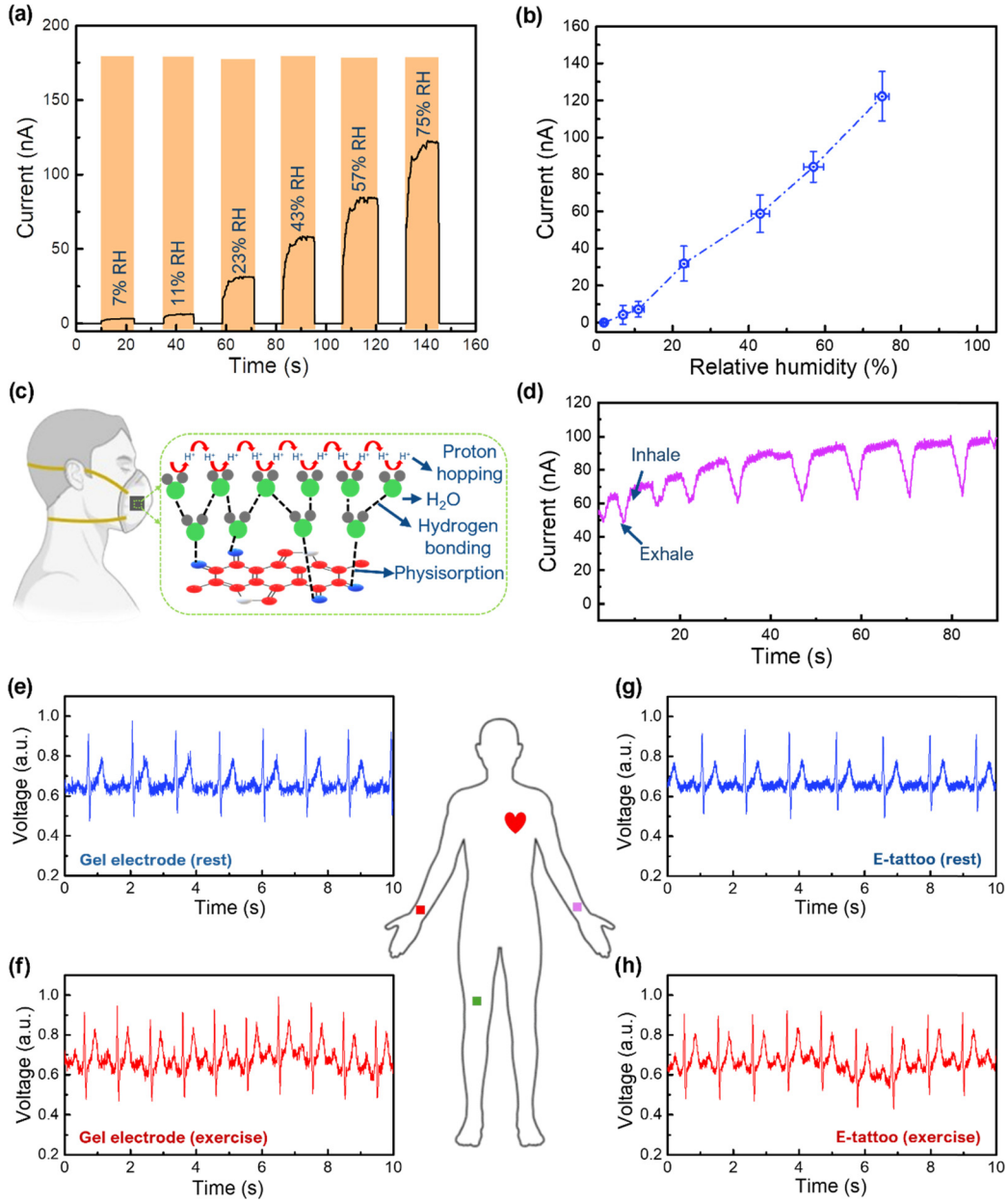

Fig. 5 Humidity sensing and electrophysiological signal monitoring. (a) Current *versus* time (*C*–*T*) curve showing the change in current with increasing humidity across the melanin-doped SNF mat. (b) Variation of current with increasing humidity across the melanin-doped SNF mat. (c) Schematic representation of the melanin-doped SNF membrane integrated into a face mask for breath monitoring. (d) *C*–*T* curve depicting changes in current during exhalation and inhalation while using the facemask. ECG signals recorded using a commercial Ag/AgCl gel electrode during the (e) rest state and (f) post-physical activity. ECG signal using the E-tattoo during the (g) rest state and (h) post-physical activity.

$\sim$1.73 $\pm$ 0.13 nA/% RH, attributed to protonic conduction *via* the Grotthuss mechanism, where adsorbed water molecules form hydrogen-bonded networks, enabling efficient proton hopping.[55–57] Melanin amplifies this process by providing active proton exchange sites and increased electronic conductivity through doping by water molecules.[36] This dual-conduction mechanism accounts for the sensor's fast response at higher humidity levels.

To investigate the repeatability characteristics, the sample was exposed to 75% RH humidity for 10 consecutive cycles. As shown in Fig. S13a (ESI†), the melanin-doped SNFs exhibit adequate repeatability. The response (τ_{res}) and recovery (τ_{rec}) times of the melanin-SNF-based humidity sensor were $\sim$0.38 s and $\sim$0.52 s, respectively (Fig. S13b, ESI†), during transitions between 2% and 75% RH (Table S3, ESI†). The ultrafast dynamics are attributed to the synergistic effects of the porous SNF structure and melanin's hygroscopic nature, which facilitate rapid adsorption and desorption of water molecules.[58] This ensures quick conductivity changes during humidity transitions. The high surface area and low energy barrier for

water desorption further enhance these dynamics. The sensor exhibited consistent response-recovery cycles with negligible hysteresis due to its ultrathin structure and homogeneous melanin distribution.

To evaluate the practical viability of the developed humidity sensor for environmental monitoring, its long-term stability was tested under 75% RH conditions. Five melanin-doped SNF-based humidity sensors were examined, with their response time, recovery time, and current monitored over a two-week period. As shown in Fig. S14 (ESI†), the response and recovery times varied by ~15%, while the current fluctuation was around 10% after two weeks. This variation is likely due to structural and environmental influences affecting material stability. Additionally, conformational shifts in the silk nanofiber (SNF) matrix and alterations in hydrogen bonding interactions between melanin and silk fibroin could influence charge transport and diffusion characteristics. Prolonged exposure to high humidity levels and environmental fluctuations may also lead to microstructural fatigue or mild oxidation, contributing to changes in sensor performance. Nevertheless, it is important to highlight that despite these variations, the response and recovery times of the melanin-doped SNF-based humidity sensors remain significantly better than those determined in previously published reports (Table S3, ESI†), demonstrating their reliability for long-term sensing applications.

The melanin–SNF humidity sensor's rapid response and recovery times make it suitable for real-time respiratory monitoring. To test this, the sensor was integrated into a face mask (Fig. 5c and Fig. S15, ESI†) and used to detect humidity changes during nose breathing. Exhalation, with high humidity, increased the sensor's current response, while inhalation reduced it as dry air decreased humidity levels (Fig. 5d and Video S2, ESI†). A slight hysteresis, due to high humidity exposure and insufficient desorption time between breaths, was observed but did not affect the overall performance. These results highlight the sensor's potential for medical respiratory monitoring applications.

The performance of the melanin-doped E-tattoo for ECG monitoring was evaluated by comparing its electrical signal acquisition capabilities with commercial Ag/AgCl gel electrodes. The improved electrical conductivity due to melanin doping, coupled with the excellent conformal adhesion of the E-tattoo to skin microtopography, significantly enhances ECG signal acquisition. To benchmark its effectiveness, ECG signals recorded using the melanin-doped E-tattoo and conventional Ag/AgCl gel electrodes are presented in Fig. 5e and f and g and h, respectively. During rest conditions, the signal-to-noise ratio (SNR) of the E-tattoo (~25.12 dB) was comparable to that of Ag/AgCl electrodes (~23.58 dB), confirming the E-tattoo's ability to capture high-quality ECG signals without using conductive gels or adhesives. This performance aligns well with previously reported SNR values for dry AgNWs/PDMS electrodes[59] and flexible conductive fabrics,[60,61] confirming the high quality of ECG signals acquired by our E-tattoo. The high porosity and mechanical flexibility of the E-tattoo further facilitated stable and continuous skin contact, ensuring accurate cardiac monitoring with clearly defined PQRST waveforms, essential for clinical diagnostics. To evaluate performance under realistic scenarios, ECG recordings were conducted after 30 min of brisk walking. As anticipated, heart rates increased post-exercise; however, the clarity of the PQRST waveform remained unchanged. Under these conditions, the E-tattoo achieved an SNR of ~25.12 dB, even with minor noise from silver paste and copper wiring. A slight increase in the SNR after exercise (attributed to improved skin hydration due to perspiration) further validates its stable electrode–skin contact. To highlight the importance of melanin doping, comparative ECG measurements were conducted using an E-tattoo without melanin (Fig. S16, ESI†). This resulted in a lower SNR (~19.85 dB), demonstrating that melanin integration is crucial for effective signal acquisition. These results highlight the graphene/melanin-doped SNF E-tattoo as an effective, gel-free alternative to conventional ECG electrodes, demonstrating comparable or superior signal fidelity, improved skin adhesion, and reduced risk of irritation, thereby showcasing its practical viability for clinical bioelectronic applications.

Additionally, to evaluate skin compatibility, a 1 cm × 1 cm E-tattoo specimen and the conductive gel commonly used for ECG measurements were placed on the forearm for a duration of 24 h (Fig. S17a, ESI†). After this interval, the skin regions were carefully inspected to identify any signs of irritation (Fig. S17b, ESI†). The optical image of the forearm showed that the E-tattoo caused no adverse skin reactions. Conversely, the area treated with the gel electrode exhibited mild rashes and dryness. To perform statistical analysis, six different individuals were selected and instructed to wear both the gel electrode and the E-tattoo platform continuously for 24 h, allowing investigation of any adverse skin reactions following prolonged usage. As depicted in Fig. S17c (ESI†), none of the participants experienced discomfort, dryness, or rashes at the location of the E-tattoo. Conversely, mild rashes and dryness were observed in almost all participants at the skin regions where the gel electrodes were applied. These results demonstrate the multifunctional nature of the E-tattoo, which enables both humidity sensing and electrophysiological monitoring, highlighting its potential for next-generation biomedical and wearable health applications.

3. Conclusions

This study demonstrated multifunctional and biomaterial-based E-tattoos by utilizing melanin-doped SNFs and graphene. The graphene/melanin-doped SNF E-tattoos combine excellent biocompatibility, breathability, and mechanical flexibility with advanced sensing capabilities, offering a sustainable and skin-compatible solution for wearable bioelectronics. Their ultrathin and lightweight traits enable seamless integration with biological systems, making them suitable for imperceptible, continuous, and real-time monitoring of skin hydration, breathing, and UV irradiation. The platform's high electrical conductivity, enhanced by the melanin dopant and graphene, supports precise electrophysiological signal acquisition (ECG monitoring) with a lower noise level, comparable to commercial electrodes. The unique properties of melanin, including the

hydration-sensitive conductivity and photo-induced conductivity, coupled with graphene's superior electrical performance, create a versatile device capable of addressing key challenges in next-generation bioelectronics, advancing applications in health diagnostics, wearable sensors, and environmental monitoring.

4. Experimental section

4.1. Preparation of silk protein solution

Fresh *Bombyx mori* silk cocoons (New Hope Silkworm Farm, Gokseong-gun, South Korea) were cut into small fragments and boiled for 30 min in a 0.02 M sodium carbonate (Na_2CO_3) aqueous solution to remove the sericin protein. The degummed fibres were thoroughly washed with distilled water and then dried for 24 h. These dried fibres were dissolved in a 9.3 M lithium bromide (LiBr) solution and incubated at 60 °C for 4 h to prepare a highly viscous silk fibroin solution. The solution was dialyzed at room temperature for 48 h using a dialysis membrane (Cellu-Sep T1, Membrane Filtration Products, MWCO 3.5K) to remove the residual salts. Following dialysis, the solution was centrifuged twice at −1 °C and 9000 rpm for 20 min each to eliminate impurities. The final aqueous silk fibroin solution had a concentration of ∼6 wt% and was cooled to room temperature before being stored at 4 °C for subsequent use.

4.2. Synthesis of the SNF mat

To fabricate the electrospun SNF mat, poly(ethylene oxide) (PEO; $M_w \approx 900\,000$, Sigma-Aldrich) was incorporated into the prepared silk solution to achieve a mixture with optimal viscosity and surface tension. The primary solution was formulated by combining the silk solution and a ∼5 wt% PEO solution at a 1 : 1 volumetric ratio, followed by homogeneous mixing using a vortex mixer. The resulting silk/PEO mixture was loaded into a 10 mL Luer-lock syringe (Henke-Ject, Germany) equipped with a 25 G steel needle and mounted onto an electrospinning unit (NanoNC, ESR200R2D, South Korea). Electrospinning was performed with the needle tip positioned 15 cm from an aluminium foil-wrapped collector, while Scotch tape-attached glass slides were placed on the collector as substrates. The process was conducted at an applied voltage of 12 kV with a solution flow rate of 30 μL min^{-1} for a duration of 6 h. To render the SNFs water-insoluble, the electrospun SNFs underwent methanol treatment, promoting crystallization of the silk protein. The ultrathin SNF layer was subsequently detached from the substrate, resulting in a substrate-free porous E-tattoo template.

4.3. Fabrication of the melanin-doped SNF mat

Melanin powder (Sigma Aldrich) was dissolved in a 0.15 M NH_4OH solution at varying concentrations (0.1 wt%, 0.5 wt%, 1 wt%, 2 wt%, and 4 wt%) to prepare a stable and uniform melanin solution. The degree of melanin doping on the SNF mat was controlled by adjusting the immersion duration (30 min, 1 h, 2 h, 4 h, 8 h, 12 h, 16 h, 20 h, and 24 h). Following immersion, the samples were air-dried at room temperature for 12 h.

4.4. Humidity response of the melanin-doped SNF mat

The humidity response of the melanin-doped SNF mat was evaluated using a custom-built static humidity characterization system. This system included solenoid valves (S10MM20-24-2, Pneumadyne Inc., USA), a humidity/temperature sensor (SHT15, Sensirion), a microcontroller board (Arduino Uno, Arduino cc), and a microscope incubator (CU-501, Live Cell Instrument). The solenoid valves were controlled using LabVIEW software (National Instruments), enabling precise and automated management of the humidity conditions within the testing chamber. Dry nitrogen (N_2) gas was utilized as a carrier gas. Various saturated salt solutions were utilized to establish specific RH environments: lithium chloride (LiCl, Sigma Aldrich) for 11% RH, magnesium chloride ($MgCl_2$, Sigma Aldrich) for 33% RH, potassium carbonate (K_2CO_3, Sigma Aldrich) for 43% RH, sodium bromide (NaBr, Sigma Aldrich) for 59% RH, sodium chloride (NaCl, Sigma Aldrich) for 75% RH, potassium chloride (KCl, Sigma Aldrich) for 85% RH, and potassium sulphate (K_2SO_4, Sigma Aldrich) for 98% RH. During testing, the humidity surrounding the sample was altered by rapidly transferring it between sealed glass vials with varying RH levels. The *I–V* characteristics of the melanin–SNF-based humidity sensors were measured using a Keithley-2450 Source Meter (Keithley Instruments Inc., USA).

4.5. Fabrication of graphene/melanin-doped SNF E-tattoos

Firstly, for preparing the graphene ink, a small amount of commercially available expandable graphite (∼1 mg) was kept inside a microwave oven for ∼30 s under ambient conditions, transforming it into worm-like graphene (WLG). The WLG was then dispersed in a 33 wt% hydrogen peroxide (H_2O_2, 30 wt%, Sigma Aldrich) solution and ultrasonicated for 15 min. The dispersion was then subjected to additional microwave irradiation for ∼60 s, during which gas release facilitated the exfoliation of the material into few-layer graphene (FLG). The FLG was then dried in a vacuum oven at 100 °C for 1 h. Subsequently, 10 mg of sodium lauryl sulphate (SLS, Sigma Aldrich) was dissolved in 1 mL of methanol through ultrasonication and 1 mg of FLG was added to the solution, followed by another 3 h of ultrasonication. To enhance the solution's viscosity, 5 mg of PEO was added and continuously mixed for 7 days. The prepared graphene ink was uniformly coated onto the melanin-doped SNF mat using a paintbrush and allowed to dry at room temperature for 4 h. Once completely dried, the E-tattoo was ready for use.

4.6. ECG monitoring using the E-tattoo electrode

For ECG measurements, the E-tattoo platforms were conformally adhered to the human body. To record ECG signals, three E-tattoo electrodes were laminated onto different parts of the body. The positive electrode was positioned on the left wrist, the negative electrode on the right wrist, and the ground electrode on the right thigh. These electrodes were connected to an Arduino Uno system equipped with an ECG amplifier and an ECG sensor module (AD8232, SparkFun) to capture and process the ECG signals. The signal to noise ratio (SNR) for the obtained ECG data

was obtained using the following formula:

$$\mathrm{SNR} = 20 \times \log_{10}\left(\frac{A_{\mathrm{signal}}}{\sigma_{\mathrm{noise}}}\right) \quad (2)$$

where A_{signal} is the peak-to-peak amplitude of the ECG signal and σ_{noise} is the standard deviation of noise.

4.7. Characterization

The surface morphology and structural characteristics of the melanin-doped SNF and E-tattoo patches were examined using field emission scanning electron microscopy (FE-SEM, FC-SM40, Hitachi). Fourier transform infrared spectroscopy (FTIR, Nicolet iS50, Thermo Scientific, USA) was employed to analyse the chemical bonding between the graphene, melanin, and SNF mat. The tensile properties were evaluated using a universal testing machine (UTM, Shimadzu, Kyoto, Japan) at a crosshead speed of 0.1 mm min^{-1} in accordance with the ASTM D882 standard. The tensile test samples measured approximately 5 mm × 30 mm. The electrical properties, including *I–V* and *C–T* characteristics, were measured using a Keithley 2400 Source Measure Unit (SMU). To facilitate electrical signal application, fine copper wires (Nilaco, CU111267) were bonded to the surface of the samples using silver paste. A 365 nm UV LED (Thor Labs, USA) was utilized for photodetection measurements. The electrical impedance properties were analysed using an LCR meter (4263B, Agilent Technologies, Kobe, Hyogo, Japan). The impedance was measured at various discrete frequencies (100 Hz, 120 Hz, 1 kHz, 10 kHz, 20 kHz, and 100 kHz). To ensure accuracy, the LCR meter was calibrated according to the manufacturer's standard procedure. Five different samples were used for statistical analysis and all measurements were conducted at room temperature.

Author contributions

Shalik Ram Joshi: conceptualization, data curation, formal analysis, investigation, methodology, and writing of the original draft; Soohoon Lee: data acquisition, analysis, and investigation; and Sunghwan Kim: conceptualization, resources, project administration, supervision, funding acquisition, writing, reviewing, and editing.

Data availability

The data supporting this article have been included as part of the ESI.†

Conflicts of interest

There are no conflicts of interest to declare.

Acknowledgements

The authors would like to acknowledge support provided by the National Research Foundation of Korea (no. RS-2023-00237928).

References

1 D.-H. Kim, N. Lu, R. Ma, Y.-S. Kim, R.-H. Kim, S. Wang, J. Wu, S. M. Won, H. Tao and A. Islam, *Science*, 2011, **333**, 838–843.
2 A. Miyamoto, S. Lee, N. F. Cooray, S. Lee, M. Mori, N. Matsuhisa, H. Jin, L. Yoda, T. Yokota and A. Itoh, *Nat. Nanotechnol.*, 2017, **12**, 907–913.
3 Y. Zhang and T. H. Tao, *Adv. Mater.*, 2019, **31**, 1905767.
4 R. C. Webb, A. P. Bonifas, A. Behnaz, Y. Zhang, K. J. Yu, H. Cheng, M. Shi, Z. Bian, Z. Liu and Y.-S. Kim, *Nat. Mater.*, 2013, **12**, 938–944.
5 D. Son, J. Lee, S. Qiao, R. Ghaffari, J. Kim, J. E. Lee, C. Song, S. J. Kim, D. J. Lee, S. W. Jun, S. Yang, M. Park, J. Shin, K. Do, M. Lee, K. Kang, C. S. Hwang, N. Lu, T. Hyeon and D.-H. Kim, *Nat. Nanotechnol.*, 2014, **9**, 397–404.
6 T. Stuart, J. Hanna and P. Gutruf, *APL Bioeng.*, 2022, **6**, 021502.
7 L. B. Baker, *Temperature*, 2019, **6**, 211–259.
8 G. Cevc, *Exp. Opin. Invest. Drugs*, 1997, **6**, 1887–1937.
9 I. M. Gidado, M. Qassem, I. F. Triantis and P. A. Kyriacou, *Sensors*, 2022, **22**, 7151.
10 M. Morin, T. Ruzgas, P. Svedenhag, C. D. Anderson, S. Ollmar, J. Engblom and S. Björklund, *Sci. Rep.*, 2020, **10**, 17218.
11 N. Gogurla, Y. Kim, S. Cho, J. Kim and S. Kim, *Adv. Mater.*, 2021, **33**, 2170188.
12 W.-H. Yeo, Y.-S. Kim, J. Lee, A. Ameen, L. Shi, M. Li, S. Wang, R. Ma, S. H. Jin and Z. Kang, *Adv. Mater.*, 2013, **25**, 2773.
13 S. Liu, Y. Rao, H. Jang, P. Tan and N. Lu, *Matter*, 2022, **5**, 1104–1136.
14 M. A. Meitl, Z.-T. Zhu, V. Kumar, K. J. Lee, X. Feng, Y. Y. Huang, I. Adesida, R. G. Nuzzo and J. A. Rogers, *Nat. Mater.*, 2006, **5**, 33–38.
15 L. Wang and N. Lu, *J. Appl. Mech.*, 2016, **83**, 041007.
16 A. Pratap, N. Gogurla and S. Kim, *ACS Appl. Electron. Mater.*, 2022, **4**, 1124–1131.
17 K. Sim, Z. Rao, Z. Zou, F. Ershad, J. Lei, A. Thukral, J. Chen, Q. Huang, J. Xiao and C. Yu, *Sci. Adv.*, 2019, **5**, 9653.
18 A. Campana, T. Cramer, D. Simon, M. Berggren and F. Biscarini, *Adv. Mater.*, 2014, **26**, 3874–3878.
19 S. Kabiri Ameri, R. Ho, H. Jang, L. Tao, Y. Wang, L. Wang, D. M. Schnyer, D. Akinwande and N. Lu, *ACS Nano*, 2017, **11**, 7634–7641.
20 P. Laux, T. Tralau, J. Tentschert, A. Blume, S. Al Dahouk, W. Bäumler, E. Bernstein, B. Bocca, A. Alimonti and H. Colebrook, *Lancet*, 2016, **387**, 395–402.
21 J. Choi and S. Kim, *ACS Biomater. Sci. Eng.*, 2023, **9**, 6390–6397.
22 S. R. Joshi, A. Pratap, N. Gogurla and S. Kim, *Adv. Electron. Mater.*, 2023, **9**, 2201095.
23 T. Y. Lee, J. Choi, S. Lee, H. Jeon and S. Kim, *Small*, 2024, **20**, 2403169.
24 S.-C. Chung, J.-S. Park, R. K. Jha, J. Kim, J. Kim, M. Kim, J. Choi, H. Kim, D.-H. Park and N. Gogurla, *ACS Appl. Mater. Interfaces*, 2022, **14**, 56623–56634.

25 J. Park, S.-G. Lee, B. Marelli, M. Lee, T. Kim, H.-K. Oh, H. Jeon, F. G. Omenetto and S. Kim, *RSC Adv.*, 2016, **6**, 39330–39334.
26 H. Tao, M. A. Brenckle, M. Yang, J. Zhang, M. Liu, S. M. Siebert, R. D. Averitt, M. S. Mannoor, M. C. Mcalpine and J. A. Rogers, *Adv. Mater.*, 2012, **24**, 1067–1072.
27 S. H. Kim, Y. S. Nam, T. S. Lee and W. H. Park, *Polym. J.*, 2003, **35**, 185–190.
28 Z. Chen and C. Lu, *Sens. Lett.*, 2005, **3**, 274–295.
29 J. Andreu-Perez, D. R. Leff, H. M. D. Ip and G.-Z. Yang, *IEEE Trans. Biomed. Eng.*, 2015, **62**, 2750–2762.
30 V. Kafil, B. Sreenan, M. Hadj-Nacer, Y. Wang, J. Yoon, M. Greiner, P. Chu, X. Wang, M. S. Fadali and X. Zhu, *Sens. Actuators, A*, 2024, **373**, 115440.
31 S. Aftab, A. A. Al-Kahtani, M. Z. Iqbal, S. Hussain and G. Koyyada, *Adv. Mater. Technol.*, 2023, **8**, 2202168.
32 H. Wang, S. Li, H. Lu, M. Zhu, H. Liang, X. Wu and Y. Zhang, *Small Methods*, 2023, **7**, 2201340.
33 S. Premi, S. Wallisch, C. M. Mano, A. B. Weiner, A. Bacchiocchi, K. Wakamatsu, E. J. Bechara, R. Halaban, T. Douki and D. E. Brash, *Science*, 2015, **347**, 842–847.
34 A. B. Mostert, S. B. Rienecker, C. Noble, G. R. Hanson and P. Meredith, *Sci. Adv.*, 2018, **4**, 1293.
35 W. Cao, X. Zhou, N. C. Mccallum, Z. Hu, Q. Z. Ni, U. Kapoor, C. M. Heil, K. S. Cay, T. Zand and A. J. Mantanona, *J. Am. Chem. Soc.*, 2021, **143**, 2622–2637.
36 M. Sheliakina, A. B. Mostert and P. Meredith, *Adv. Funct. Mater.*, 2018, **28**, 1805514.
37 S. R. Joshi, M. Lee, H. Y. Lee, M.-E. Lee and S. Kim, *Chem. Eng. J.*, 2024, **496**, 154160.
38 F. Ahmad, M. Zahid, H. Jamil, M. A. Khan, S. Atiq, M. Bibi, K. Shahbaz, M. Adnan, M. Danish and F. Rasheed, *J. Energy Storage*, 2023, **72**, 108731.
39 S. Bhattacharya, M. Nikbakht, A. Alden, P. Tan, J. Wang, T. A. Alhalimi, S. Kim, P. Wang, H. Tanaka and A. Tandon, *Adv. Electron. Mater.*, 2023, **9**, 2201284.
40 M. Jo, K. Min, B. Roy, S. Kim, S. Lee, J.-Y. Park and S. Kim, *ACS Nano*, 2018, **12**, 5637–5645.
41 Y. Ikemoto, Y. Harada, M. Tanaka, S. Nishimura, D. Murakami, N. Kurahashi, T. Moriwaki, K. Yamazoe, H. Washizu, Y. Ishii and H. Torii, *J. Phys. Chem. B*, 2022, **126**, 4143–4151.
42 Z. Çiplak, N. Yildiz and A. Çalimli, *Fullerenes, Nanotubes Carbon Nanostruct.*, 2015, **23**, 361–370.
43 I. Faniyi, O. Fasakin, B. Olofinjana, A. Adekunle, T. Oluwasusi, M. Eleruja and E. Ajayi, *Appl. Sci.*, 2019, **1**, 1–7.
44 B.-G. Cho, S. R. Joshi, S. Lee, S.-K. Kim, Y.-B. Park and G.-H. Kim, *Polymers*, 2021, **13**, 615.
45 B.-G. Cho, S. R. Joshi, J. H. Han, G.-H. Kim and Y.-B. Park, *Composites, Part A*, 2021, **149**, 106521.
46 C. Wan, Z. Wu, M. Ren, M. Tang, Y. Gao, X. Shang, T. Li, Z. Xia, Z. Yang, S. Mao, M. Zhou, W. Ling, J. Li, W. Huo and X. Huang, *ACS Nano*, 2023, **17**, 10689–10700.
47 S. Yang and X. Jiang, *ACS Nano*, 2024, **18**(40), 27107–27125.
48 Y. Chen, G. Zhou, X. Yuan, C. Li, L. Liu and H. You, *Biosens. Bioelectron.*, 2022, **206**, 114118.
49 R. Matsukawa, A. Miyamoto, T. Yokota and T. Someya, *Adv. Healthcare Mater.*, 2020, **9**, 2001322.
50 I. Chatterjee, D. Wu and O. P. Gandhi, *IEEE Trans. Biomed. Eng.*, 1986, **33**, 486–494.
51 K. Goyal, D. A. Borkholder and S. W. Day, *Sensors*, 2022, **22**, 8510.
52 B. K. Armstrong and A. Kricker, *J. Photochem. Photobiol., B*, 2001, **63**, 8–18.
53 S. Cai, X. Xu, W. Yang, J. Chen and X. Fang, *Adv. Mater.*, 2019, **31**, 1808138.
54 Z. Zhu, Y. Gu, S. Wang, Y. Zhou and H. Zheng, *Adv. Electron. Mater.*, 2017, **3**, 1700281.
55 Z. V. Bedran, S. S. Zhukov, P. A. Abramov, I. O. Tyurenkov, B. P. Gorshunov, A. B. Mostert and K. A. Motovilov, *Polymers*, 2021, **13**, 4403.
56 M. Matta, A. Pezzella and A. Troisi, *J. Phys. Chem. Lett.*, 2020, **11**, 1045–1051.
57 H. Farahani, R. Wagiran and M. N. Hamidon, *Sensors*, 2014, **14**, 7881–7939.
58 S. R. Joshi, B. Kim, S.-K. Kim, W. Song, K. Park, G.-H. Kim and H. Shin, *J. Electrochem. Soc.*, 2020, **167**, 147511.
59 R. R. Kisannagar, P. Jha, A. Navalkar, S. K. Maji and D. Gupta, *ACS Omega*, 2020, **5**(18), 10260–10265.
60 A. Joutsen, A. Cömert, E. Kaappa, K. Vanhatalo, J. Riistama, A. Vehkaoja and H. Eskola, *Sci. Rep.*, 2024, **14**, 8882.
61 J. Ferri, R. Llinares, I. Segarra, A. Cebrián, E. Garcia-Breijo and J. Millet, *Electrochem. Commun.*, 2022, **136**, 107244.

